A&A 515, A57 (2010)
DOI: 10.1051/0004-6361/200912078

Astronomy & Astrophysics

New measurements of radial velocities in clusters of galaxies-V⋆,⋆⋆

D. Proust[1], H. V. Capelato[2], G. B. Lima Neto[3], and L. Sodré Jr.[3]

[1] Observatoire de Paris-Meudon, GEPI, 92195 Meudon, France
e-mail: dominique.proust@obspm.fr
[2] Divisão de Astrofísica, INPE/MCT, 12227-010 São José dos Campos/S.P., Brazil
[3] Instituto de Astronomia, Geofísica e Ciências Atmosfericos, Universidade de São Paulo (IAG/USP), 05508-090 São Paulo/S.P., Brazil

Received 16 March 2009 / Accepted 5 February 2010

ABSTRACT

As a part of our galaxy-cluster redshift survey, we present a set of 79 new velocities in the 4 clusters Abell 376, Abell 970, Abell 1356, and Abell 2244, obtained at Haute-Provence observatory. This set now completes our previous analyses, especially for the first two clusters. Data on individual galaxies are presented, and we discuss some cluster properties. For A376, we obtained an improved mean redshift $\overline{z} = 0.04750$ with a velocity dispersion of $\sigma_V = 860$ km s^{-1}. For A970, we have $\overline{z} = 0.05875$ with $\sigma_V = 881$ km s^{-1}. We show that the A1356 cluster is not a member of the "Leo-Virgo" supercluster at a mean redshift $\overline{z} = 0.112$ and should be considered just as a foreground group of galaxies at $\overline{z} = 0.0689$, as well as A1435 at $\overline{z} = 0.062$. We obtain $\overline{z} = 0.09962$ for A2244 with $\sigma_V = 965$ km s^{-1}. The relative proximity of clusters A2244 and A2245 ($\overline{z} = 0.08738$, $\sigma_V = 992$ km s^{-1}) suggests that these could be members of a supercluster that would include A2249; however, from X-ray data there is no indication of interaction between A2244 and A2245.

Key words. galaxies: distances and redshifts – galaxies: cluster: general – galaxies: clusters: individual: Abell 376 – galaxies: clusters: individual: Abell 970 – galaxies: clusters: individual: Abell 1356 – galaxies: clusters: individual: Abell 2244

1. Introduction

Redshift surveys in clusters of galaxies are needed to study their dynamical and evolutionary state. In clusters, the mean velocity is a key factor in deriving distances, allowing the study of matter distribution on very large scales. Within clusters analysis of the velocity field can lead to an estimate of the virial mass, constraining models of the dark matter content. Galaxy velocity measurements provide informations that are complementary to other wavelengths, in particular what are obtained through X-ray observations of clusters. Optical, spectroscopic, and X-ray data form basic pieces of information for the mass estimates. However, discrepancies between these estimators are often found (e.g. Girardi et al. 1998; Allen 2000; Cypriano et al. 2005). Virial mass estimates rely on the assumption of dynamical equilibrium. X-ray mass estimates also depend on the dynamical equilibrium hypothesis and on the still not well-constrained intracluster gas temperature gradient (e.g., Leccardi & Molendi 2008). Finally, mass estimates based on gravitational lensing are considered more reliable than the others (e.g., Mellier 1999) because they are completely independent of the dynamical status of the cluster. The drawback is that lensing can only probe the central region of clusters. The discrepancies among the methods may come from the non-equilibrium effects in the central region of the clusters (Allen 1998).

In this paper, we complete our preceeding studies of the dynamical status of the two clusters Abell 376 (Proust et al. 2003) and Abell 970 (Sodré et al. 2001; Lima Neto et al. 2003) with the addition of 46 and 14 galaxies, respectively. The observations of radial velocities reported here are part of a program to study the dynamical structure of clusters of galaxies, which was started years ago and which had several already published analyses (see e.g. Proust et al. 1992, 1995, 2000; Capelato et al. 1991, 2008, and references above).

We have added only 10 galaxies in each of the two clusters Abell 1356 and Abell 2244 since a larger set of velocities in these two clusters have been obtained in the course of the Sloan Digital Sky Survey (SDSS)[1]. For that reason spectroscopic observations were no longer pursued in these two clusters.

We present in Sect. 2 the details of the observations and data reduction. In Sect. 3 we discuss the distribution and the velocity analysis of the cluster galaxies, and we summarize our conclusions for each cluster. We adopt here, whenever necessary, $H_0 = 70\,h_{70}$ km s^{-1} Mpc^{-1}, $\Omega_M = 0.3$ and $\Omega_\Lambda = 0.7$.

2. Observations and data reductions

The new velocities presented in this paper were obtained with the 1.93m telescope at Haute-Provence Observatory. Observations were carried out in April 2000, May 2001 and January 2005. We used the CARELEC spectrograph at the Cassegrain focus, equipped with a 150 line/mm grating blazed at 5000 Å and coupled to an EEV CCD detector 2048 × 1024 pixels with a pixel size of 13.5 μm. A dispersion of 260 Å/mm was used, providing spectral coverage from 3600 to 7300 Å. Wavelength calibration was done using exposures of He-Ne lamps.

⋆ Based on observations made Haute-Provence observatory (France).
⋆⋆ Table 1 is also available in electronic form at the CDS via anonymous ftp to cdsarc.u-strasbg.fr (130.79.128.5) or via http://cdsweb.u-strasbg.fr/cgi-bin/qcat?J/A+A/515/A57

[1] http://www.sdss.org/

The data reduction was carried out with IRAF[2] using the LONGSLIT package. Radial velocities were determined using the cross-correlation technique (Tonry & Davis 1979) implemented in the RVSAO package (Kurtz et al. 1991; Mink et al. 1995) with radial velocity standards obtained from observations of late-type stars and previously well studied galaxies.

A total of 79 velocities was obtained from our observations. Table 1 lists positions and heliocentric velocities for individual galaxies with the following columns:

1. number of the object. For A376, this number refers to Dressler (1980) and for A970 it continues the list of Sodré et al. (2001);
2. right ascension (J2000);
3. declination (J2000);
4. morphological type either from Dressler's (1980) catalog for A376 and from a visual inspection on the Palomar Sky Survey (POSS) for A970;
5. heliocentric radial velocity with its error in km s^{-1};
6. *R*-value derived from Tonry & Davis (1979);
7. notes.

We searched in the NED database[3] for additional velocities to complement our redshift samples. As mentioned before, the fields of A1356 and A2244 are within the sky coverage area of the Sloan Digital Sky Survey, and because of that most of the 20 measurements made for these clusters resulted in duplicated data: only 5 new redshifts could have contributed to A1356 and none for A2244. This last cluster was studied by Rines & Diaferio (2006) using the caustics technic (Diaferia 1999) to remove interlopers and to estimate the velocity dispersions within r_{200}. We have no more information to add to their work.

For already observed galaxies, velocity comparison was made between our data set and NED. We obtained $\langle V_o - V_{ref} \rangle = 31$ km s^{-1}, the standard deviation of the difference being 67 km s^{-1}. These results are consistent with the errors of Table 1. The velocities in the present study agree with those previously published within the 2σ level.

3. Galaxy distribution and kinematical analysis

3.1. Abell 376

When including previous measurements (Proust et al. 2003, hereafter P03), there is a total of 113 measured velocities in the field of Abell 376, from which 40 are new ones. Note that galaxies from our redshift sample were selected from the the morphological sample of A376 by Dressler (1980), being almost complete (113 out of 120). As in P03, galaxy photometry were provided by the POSS I Revised APS Catalogue[4] (Cabanela et al. 2003) which gives integrated magnitudes in the blue photographic *O* band. Figure 1, which is equivalent to Fig. 1 of P03, shows the projected distribution of galaxies in the field of Abell 376, where galaxies with measured redshifts have been identified.

[2] IRAF is distributed by the National Optical Astronomy Observatories, which are operated by the Association of Universities for Research in Astronomy, Inc., under cooperative agreement with the National Science Foundation.

[3] The NASA/IPAC Extragalactic Database (NED) is operated by the Jet Propulsion Laboratory, California Institute of Technology, under contract with the National Aeronautics and Space Administration.

[4] The POSS-I Revised APS Catalogue is available at the MAPS database from the University of Minnesota, at http://aps.umn.edu/

Table 1. Heliocentric redshift, position, and morphological type for galaxies of A376, A970, A1356, and A2244.

Galaxy id.	RA (2000)	Dec (2000)	Type	Hel. Vel. $V \pm \Delta V$	*R*	*N*
A376						
1	02 46 29.0	+36 27 19	S	40 451 32	6.53	1
4	02 46 21.0	+36 30 43	E	39 967 26	5.93	2
10	02 46 40.5	+36 35 44	S0	36 533 49	3.08	
12	02 46 25.4	+36 34 48	S0	13 881 59	3.98	
13	02 46 25.3	+36 32 24	S	15 026 61	5.69	l1
14	02 45 47.0	+36 35 57	S	13 526 127	3.05	
15	02 45 07.6	+36 36 49	S0	14 018 74	5.03	
16	02 45 06.7	+36 34 02	S	12 977 68	4.49	3
17	02 44 43.9	+36 35 46	E/S0	13 638 101	3.22	
19	02 46 47.6	+36 40 38	S0	13 629 108	3.01	weak
21	02 45 55.6	+36 43 14	S0	14 873 53	3.68	l2
23	02 45 32.6	+36 40 46	S	13 398 29	10.65	4
29	02 44 52.5	+36 40 21	S	15 602 68	3.35	
30	02 44 16.2	+36 44 00	S	41 071 50	3.79	5
38	02 46 25.0	+36 48 37	E	13 975 131	3.76	
39	02 46 20.5	+36 46 20	E/S0	15 415 100	3.39	
46	02 44 58.9	+36 45 54	S	14 401 49	4.25	l3
47	02 44 53.9	+36 47 32	Ep	14 514 60	3.29	l4
48	02 44 44.5	+36 45 00	I	14 702 56	6.69	6
50	02 44 11.1	+36 45 36	S0	29 935 61	4.25	l5
51	02 43 49.1	+36 46 30	S0/E	41 546 51	5.49	
53	02 47 31.8	+36 49 45	S	13 701 21	8.87	
56	02 46 54.5	+36 53 03	E	13 897 58	4.69	l6
58	02 46 34.2	+36 54 19	S	16 215 66	4.00	l7
59	02 46 28.3	+36 51 55	S	13 310 94	3.49	
62	02 46 19.7	+36 50 52	S/I	13 772 73		7
74	02 45 48.7	+36 52 28	S0	13 466 86	3.02	weak
77	02 45 41.1	+36 52 39	S	13 553 65	3.03	
79	02 45 33.5	+36 51 43	S0	14 184 119	3.19	
80	02 45 28.8	+36 53 33	S0	14 948 118	3.02	
82	02 45 22.6	+36 50 32	S0/S	26 848 58	3.73	
83	02 45 16.5	+36 50 45	S0	15 265 35	12.35	8
87	02 44 16.6	+36 54 49	S0	12 072 78	4.03	9
99	02 45 47.9	+36 59 09	S0	13 421 63	6.41	
105	02 45 09.4	+37 00 57	S0	13 550 98	3.81	
107	02 43 54.1	+36 57 49	E/S0	14 365 81	4.28	
110	02 45 41.9	+37 06 05	E	9255 49	5.96	l8
112	02 43 51.6	+37 03 30	S	13 535 88	2.54	weak
114	02 46 08.5	+37 09 49	S	13 260 98	3.04	10
115	02 44 56.2	+37 11 56	S	44 634 76	3.02	
116	02 44 14.2	+37 09 24	E/S0	40 204 75	5.16	
117	02 44 18.8	+37 08 20	S0	40 124 74	3.10	
118	02 45 38.4	+37 18 18	S	17 561 66	4.32	11
119	02 45 38.7	+37 18 25	S0/a	14 587 55	4.29	l9
120	02 45 07.8	+37 14 24	E	14 530 53	4.49	
A970						
70	10 16 05.3	−10 57 40	E	17 014 112	3.47	
71	10 16 08.0	−10 29 49	E/S0	11 033 91	5.70	12
72	10 16 10.8	−10 28 28	S0	55 419 77	2.96	weak
73	10 16 14.0	−10 31 13	S0	17 610 116	3.07	l10
74	10 16 25.7	−10 57 43	E/S0	18 009 154	3.01	l11
75	10 16 31.9	−10 37 45	S0	12 360 93	3.66	l12
76	10 16 39.8	−10 59 59	E	15 662 94	6.18	l13
77	10 16 41.3	−10 59 03	S0/S	47 793 60	3.04	
78	10 17 17.5	−11 07 50	S0	17 709 83	4.26	
79	10 18 53.9	−10 49 25	S	19 173 17		13
80	10 18 59.0	−10 54 02	E	2701 23		14
81	10 19 09.6	−10 58 39	S	19 404 32		15
82	10 19 13.7	−10 22 31	E	33 248 50	3.32	
83	10 19 16.2	−10 22 09	S0/S	16 887 111	3.01	weak

Table 1. Continued.

Galaxy id.	RA (2000)	Dec (2000)	Type	Hel. Vel. $V\pm\Delta V$	R	N
A1356						
1	11 42 04.8	+10 21 49	S	6395 43	5.19	l14
2	11 42 08.7	+10 27 19	S	21 030 82	3.63	
3	11 42 15.3	+10 26 50	E	35 166 27	11.75	l15
4	11 42 22.3	+10 44 19	S	23 753 45	8.93	l16
5	11 42 23.7	+10 26 09	E	21 474 54	6.96	16 l29
6	11 42 24.4	+10 40 04	S	23 794 79	6.70	l17
7	11 42 29.6	+10 29 24	S	20 910 75	6.27	
8	11 42 29.7	+10 28 31	S0	20 702 51	10.56	l18
9	11 42 31.7	+10 25 24	S	10 655 75	5.61	17 l30
10	11 42 43.4	+10 31 00	E	36 132 74	3.62	weak l31
A2244						
1	17 02 16.7	+33 58 49	S	29 626 39	10.37	l19
2	17 02 25.9	+33 59 54	S0	29 062 32	11.18	l20
3	17 02 42.5	+34 03 38	S0	29 811 46	9.50	l21
4	17 02 45.6	+34 03 39	?	27 984 66	8.67	l22
5	17 03 23.5	+34 06 49	S	11 080 25	12.40	18 l23
6	17 04 03.3	+33 55 19	S	11 144 39	10.96	l24
7	17 04 04.1	+34 15 29	S0	30 606 73	6.83	l25
8	17 04 14.4	+34 15 03	S	12 180 80	6.39	19 l26
9	17 04 45.9	+34 06 34	S0	30 707 58	8.76	l27
10	17 04 50.1	+34 05 29	S	9959 58	7.29	20 l28

Notes. Data from NED:
l1 15 130 km s^{-1}; **l2** 14 958 km s^{-1}; **l3** 14 590 km s^{-1}; **l4** 14 466 km s^{-1}; **l5** 29 892 km s^{-1}; **l6** 13 988 km s^{-1}; **l7** 16 273 km s^{-1}; **l8** 9324 km s^{-1}; **l9** 14 765 km s^{-1}; **l10** 17 631 km s^{-1}; **l11** 18 067 km s^{-1}; **l12** 12 098 km s^{-1}; **l13** 15 782 km s^{-1}; **l14** NGC 3819 6274 km s^{-1}; **l15** 35 155 km s^{-1}; **l16** 23 768 km s^{-1}; **l17** 23 789 km s^{-1}; **l18** 20 773 km s^{-1}; **l19** 29 585 km s^{-1}; **l20** 29 046 km s^{-1}; **l21** 29 652 km s^{-1}; **l22** 27 955 km s^{-1}; **l23** 11 121 km s^{-1}; **l24** 11 156 km s^{-1}; **l25** 30 655 km s^{-1}; **l26** 12 110 km s^{-1}; **l27** 30 809 km s^{-1}; **l28** 9908 km s^{-1}; **l29** 21 288 km s^{-1}; **l30** 10 601 km s^{-1}; **l31** 36 047 km s^{-1}.

1 emission line: Hα = 40 498 km s^{-1}; **2** emission line: Hα = 39 982 km s^{-1}; **3** emission line: Hα = 13 072 km s^{-1}; **4** emission line: Hβ, 2OIII, Hα, $S2$; **5** emission line: Hα = 41 167 km s^{-1}; **6** emission line: Hα = 14 829 km s^{-1}; **7** emission line: OII, Hβ, 2OIII, Hα, $S1$; **8** emission line: Hα, $S2$ = 15 478 km s^{-1}; **9** emission line: Hα = 12 066 km s^{-1}; **10** emission line: Hα = 13 267 km s^{-1}; **11** emission line: Hα = 17 652 km s^{-1}; **12** emission line: Hα = 11 058 km s^{-1}; **13** emission line: Hα; **14** emission lines: 2OIII, Hα, $S1$; **15** emission line: Hα; **16** emission lines: OII, OIII, Hα, $N2$ = 21 398 ± 68 km s^{-1}; **17** emission lines: 2OIII, Hα = 10 684 ± 35 km s^{-1}; **18** emission lines: Hα, $N2$; **19** emission line: Hα; **20** emission lines: Hβ, 2OIII, Hα, $N1$, $N2$, $S1$, $S2$.

We estimated the completeness level of the redshift sample by considering the minimum rectangular area subtending the entire redshift sample. We find that the completeness reaches a maximum of only 57% at 18 mag. If considering, however, the same (rectangular) central region previously studied in P03 (see Fig. 1), the completeness level increases to a maximum of 67% at 18 mag, which is more acceptable. In view of this, we restrain the kinematical analysis to the same central region as was studied in P03. Moreover, as discussed in P03, despite its incompleteness, the 19.5 mag sample was found to be representative of the spatial distribution of galaxies in the central region of the cluster. This allows a more detailed kinematical analysis of central region of the cluster.

We used the ROSTAT routines (Beers et al. 1990; Bird & Beers 1993) to analyze the velocity distribution of our sample.

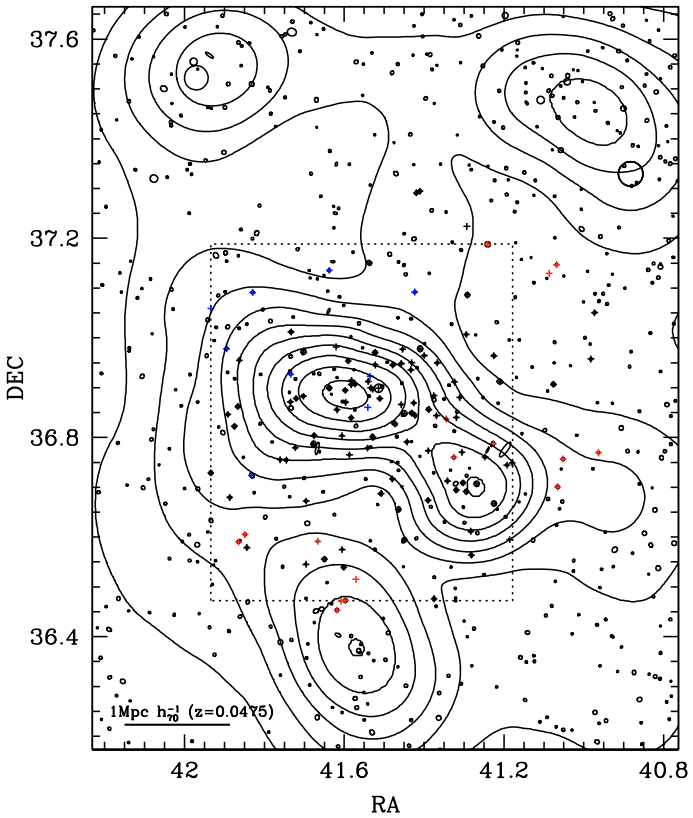

Fig. 1. Adaptative kernel density map of the 168 galaxies brighter than O = 18 projected in the field of Abell 376. The positions of galaxies brighter than O = 19.5 are plotted as ellipses of diameters, ellipticities and position angles taken from the APS catalog. Galaxies having measured redshifts are marked with pluses: blue for foreground galaxies and red for background ones.

We applied the method of the weighted gap analysis as discussed by Ribeiro et al. (1998; see also Capelato et al. 2008) in order to remove interlopers and to identify the main kinematical structures. Figure 2 (inset) shows the radial velocity distribution of the whole redshift sample, where the presence of a very dominant kinematical structure is confirmed by the gap analysis. This kinematical structure, which we identify for A376, is displayed in the main part of Fig. 2. It is constituted of 89 galaxies with radial velocities ranging between 12 500 and 16 300 km s^{-1}, with mean $\overline{V}_{\rm rec}$ = 14 241$^{+151}_{-172}$ km s^{-1}, corresponding to redshift z_{A376} = 0.04750. The velocity dispersion corrected following Danese et al. (1980) is $\sigma_{\rm corr}$ = 830$^{+122}_{-90}$ km s^{-1}[5].

The ROSTAT routines detect a significant gap (indicated by an arrow in Fig. 2) $\Delta V \sim 100$ km s^{-1} in the velocity distribution sample at $V_{\rm gap} \sim 14\,500$ km s^{-1} (3% probability of being drawn from an underlying normal distribution). To see if this reflects some special feature of the galaxy distribution, in Fig. 3 (left panel) we show the kernel weighted local mean velocity map for galaxies belonging to the kinematical structure shown in Fig. 2, together with their adaptative kernel projected density map.

As seen from this figure, the high-velocity galaxies, $V > V_{\rm gap}$, are almost completely concentrated to the north of the cluster center, characterizing an SW-NE velocity gradient, possibly caused by a substructure being accreted by the main cluster. This

[5] In this paper means and dispersions are given as biweighted estimates, see Beers et al. (1990). Error bars are 90% confidence intervals and are calculated by bootstrap re-sampling of 10 000 subsamples of the velocity data.

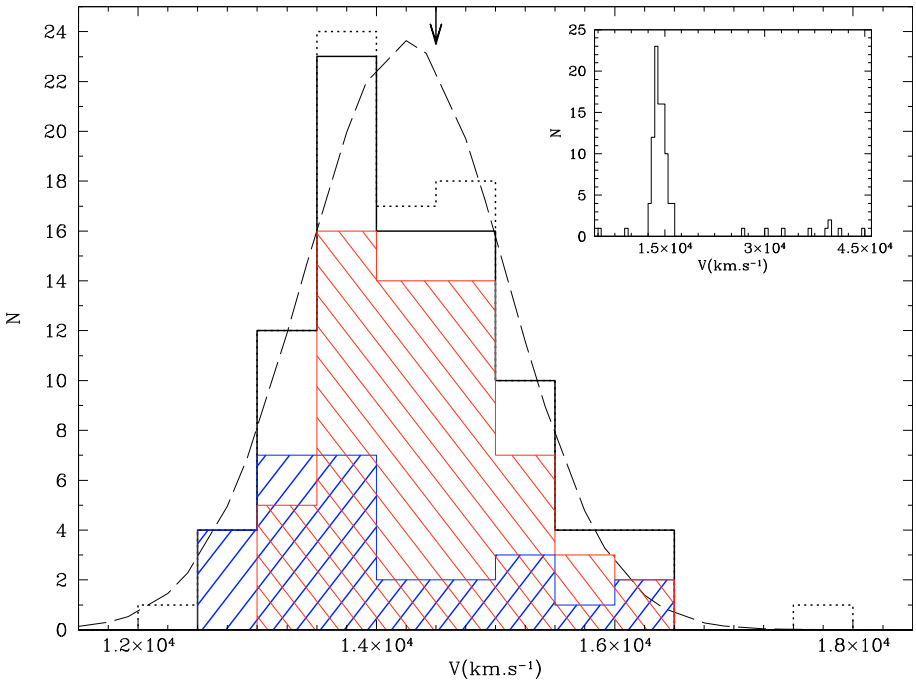

Fig. 2. The radial velocity distribution for the Abell 376 sample of galaxies between 12 000 and 18 000 km s^{-1} contained in the central region indicated in Fig. 1. The dashed line curve shows the Gaussian distribution corresponding to the mean velocity and velocity dispersion quoted in the text (normalized to the sample size). The inset show the distribution for the entire sample of 113 redshifts in the region of A376 (dotted line histogram in the main figure). The arrow indicates the position of a gap in the velocity distribution (see text). The shaded histograms show the radial velocity distributions of the E+S0 galaxies (left-handed shade; red lines) and for the S+I galaxies (right hand shade; blue lines).

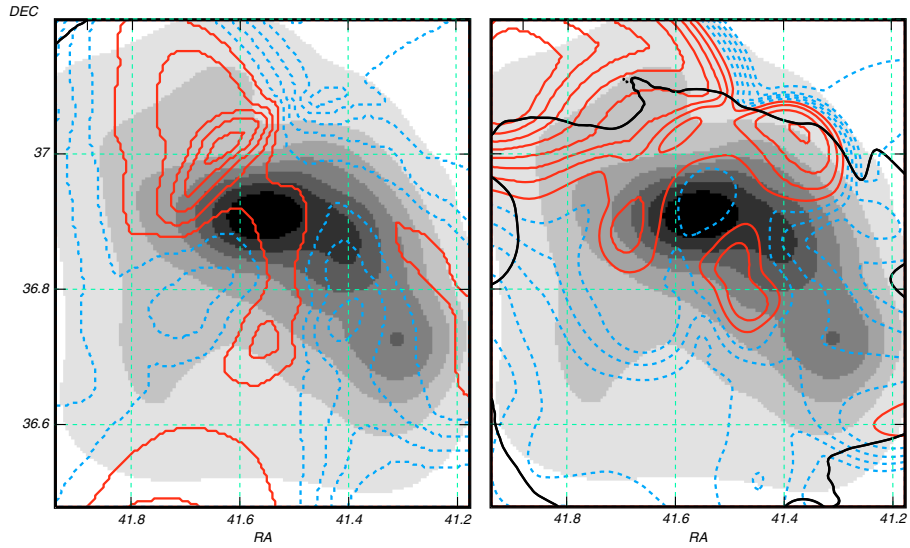

Fig. 3. Contours of equal local mean velocity (*left panel*) and of local mean dispersion velocity (*right panel*), superimposed on the gray-level AK surface density image of the central region indicated in Fig. 1. Higher values are shown with red continuous lines: $\overline{V}_{\rm rec}$ (Δ = 200 km s^{-1}) between 14 500 and 15 500 km s^{-1} (*left*) and $\overline{\sigma}$ (Δ = 100 km s^{-1}) between 900 and 1600 km s^{-1} (*right*); lower values with blue dotted lines: $\overline{V}_{\rm rec}$ between 12 500 and 14 300 km s^{-1} (*left*) and $\overline{\sigma}$ between 400 and 800 km s^{-1} (*right*). The bold black line in the left panel is the boundary of the region where results are 3σ−significant after 10 000 bootstraps of the data. All samples are limited at 19.5 mag.

suggests that the velocity distribution is bimodal. Indeed, the normality tests of ROSTAT already indicate that the distribution is assymetrically tailed, as is also apparent in Fig. 2. Figure 4 shows the local mean velocity profile taken along the line of highest gradient. As seen, the velocity gradient only manifests itself outside the core region of A376, which displays a uniform mean velocity, very nearly the same as the E/D dominant galaxy (indicated by the left arrow). This is interesting because, as noted in P03, when compared to the cluster baricenter, the peculiar velocity of the dominant galaxy (322 km s^{-1}) is only barely consistent with the distribution of peculiar velocities of cD galaxies given by Oegerle & Hill (2001). Our new analysis suggests that A376 is a far more complex structure in which only the main central core seems to conform to the properties of a (classical) relaxed cluster, thought to be centered on a large dominating spheroidal galaxy at rest relative to it.

Considering the velocity distribution of galaxies accordingly to their morphological types, Fig. 2 shows the velocity distribution of early type (E+S0: 61 objects) and late type (S+I: 28 objects) galaxies, according to the classification given by Dressler (1980). Both samples are limited at 19.5 mag. Their mean velocities and velocity dispersions are $\overline{V}_{\rm early}$ = 14 378 ± 167 km s^{-1} and $\sigma_{\rm early}$ = 716^{+133}_{-96} km s^{-1}, and for S+I types $\overline{V}_{\rm late}$ = $13\,849^{+481}_{-390}$ km s^{-1}, $\sigma_{\rm late}$ = 966^{+316}_{-297} km s^{-1}. As observed in most clusters (Sodré et al. 1989; Stein 1997; Carlberg et al. 1997; Adami et al. 1998), the velocity dispersion of the late-type population is larger than that of the early-type population. The results obtained in P03 remain unchanged with these new data.

To examine the relative contribution of early and late type galaxies to the overall projected distribution of galaxies, we show the high and low density isopleths of their distributions in Fig. 5 (left and right panels, respectively) superimposed on the AK surface density image of the photometric sample, limited at 19.5 mag. Early type galaxies are largely dominant over late-type galaxies by more than a factor 2 in number. As seen from this figure, they are also much more concentrated (dense) in the center of the cluster, by a factor ∼6. This is a clear demonstration

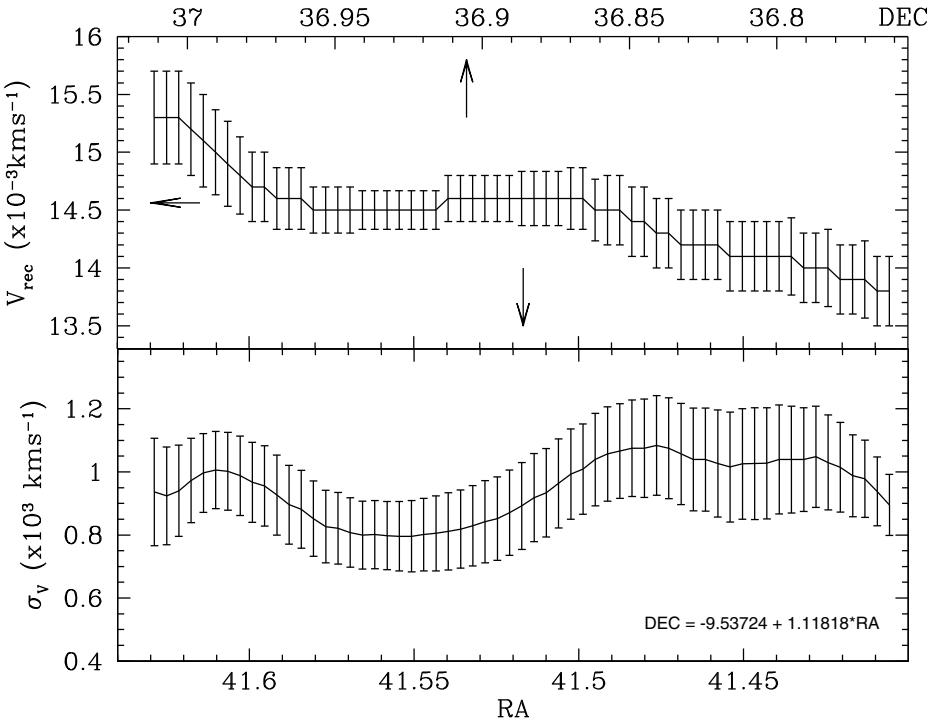

Fig. 4. The local mean velocity profile (*upper panel*) and the local dispersion velocity profile (*lower panel*) taken along a line showing the highest velocity gradient (equation given in the *lower panel*). The arrows indicate the position and velocity of the dominant E/D central cluster galaxy: lower and upper arrows for the RA and Dec positions and the left upper arrow for its velocity. Error bars are 1-σ standard deviation of mean values after 5000 data bootstraps.

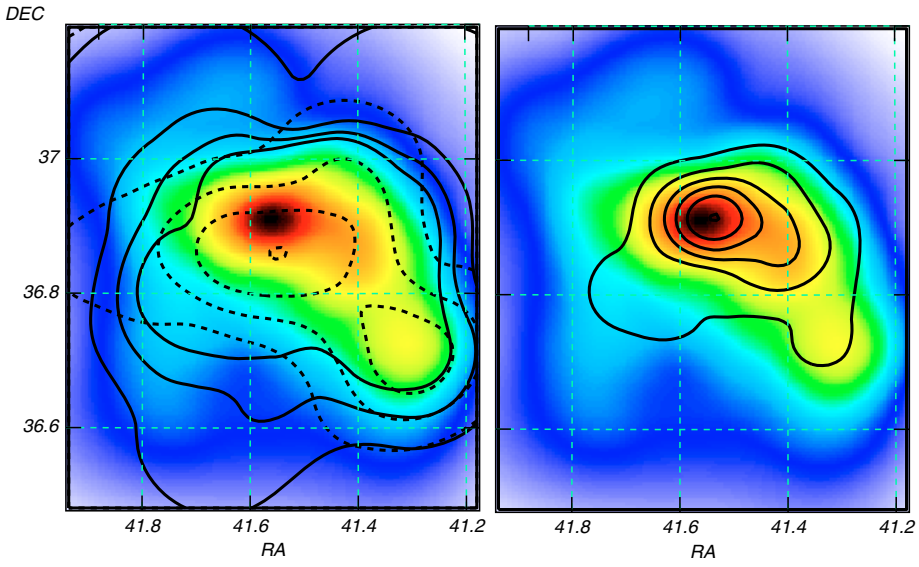

Fig. 5. Isopleths of the surface distribution of early (E+S0) galaxies (continuous lines) and late (S+I) galaxies (dotted lines) superimposed on the AK surface density image of the central region of Fig. 1. *Left panel*: low-density isopleths $\Sigma_5 < 1.4$, $\Delta_5 = 0.35$. *Right panel*: high-density isopleths $8.3 > \Sigma_5 > 1.4$, $\Delta_5 = 1.38$. Σ_5 is measured in units of 10^{-5} gal arcsec^{-2}.

of the effect of morphological segregation acting locally in the cluster.

3.2. Abell 970

This cluster is extensively discussed in Sodré et al. (2001, hereafter S01) and in Lima Neto (2003), which have shown that this is a rather complex system. Including the already published velocities (S01), 14 new redshifts for a total of 83 have been obtained in the direction of Abell 970.

As already done in S01, both the iterative gap analysis and the statistical tests provided by ROSTAT were applied to remove contaminant interloppers in the redshift sample. This has shown that the cluster radial velocities range between ~15 000 km s^{-1} and 20 000 km s^{-1}, with mean and dispersion velocities $\overline{V}_{\rm rec} = 17\,612^{+189}_{-182}$ km s^{-1} ($z_{\rm clus} = 0.05875$) and $\sigma = 881^{+144}_{-123}$ km s^{-1}. The histogram of the velocity distribution is displayed in Fig. 6.

These analyses have also shown a significant gap in the velocity distribution, $V_{\rm gap} \sim 18\,500$ km s^{-1}, already reported by S01 (see Fig. 6). In that work it was suggested that the gap occured because of the bimodality of the radial velocity distribution, signaling the state of non equilibrium of the cluster, also proven by the presence of very compact clump of galaxies situated ~8 arcmin ($544\,h_{70}^{-1}$ Kpc at $z = 0.059$) NW of the BCG with mean velocity $\overline{V}_{\rm clump} = 19\,227$ km s^{-1}. The new data presented here reinforces this picture, since the new redshifts distribute everywhere outside the central ~1 Mpc region of the cluster. The off-set of the X-ray emission distribution relative to the galaxy distribution and the gas temperature and metal abundance gradients are also strong evidence that A970 has suffered a recent merger with a subcluster or that the NW substructure has

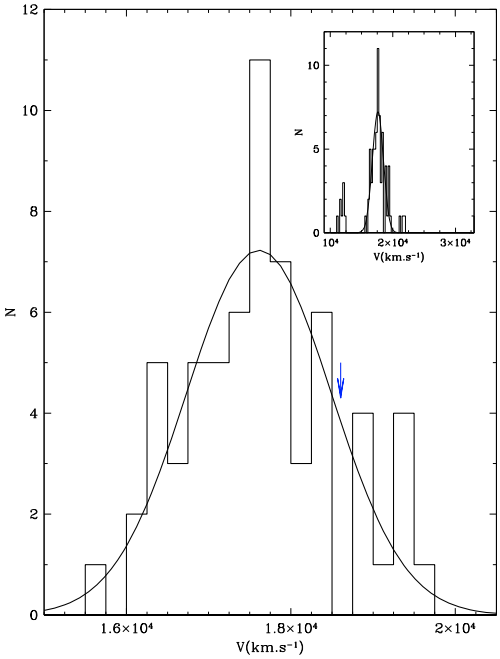

Fig. 6. The radial velocity distribution for the Abell 970 sample of galaxies between 15 000 and 20 000 km s^{-1}. The continuous curve shows the Gaussian distribution as in Fig. 2. The arrow at $v \sim 18\,600$ km s^{-1} points to a significant gap found from the gap analysis.

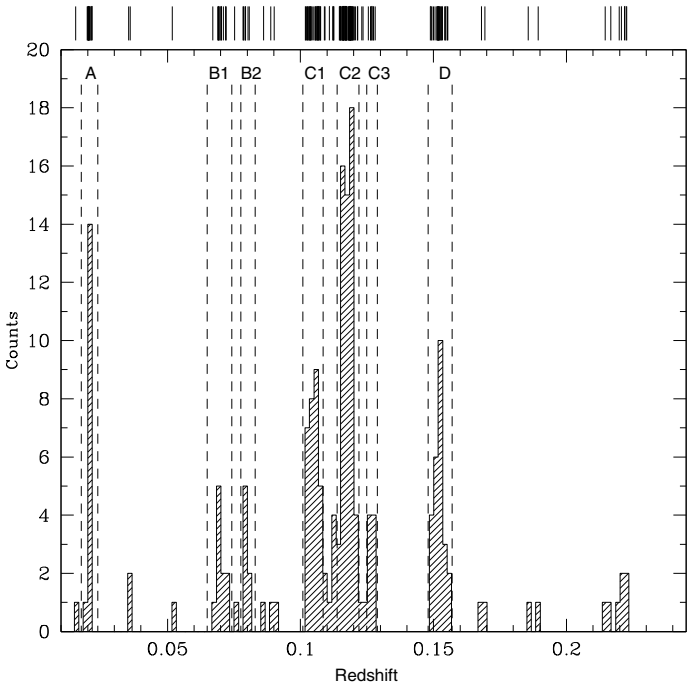

Fig. 7. The redshift distribution of a square region of 0.83° side centered on the nominal center of A1356 ($11^h42^m28.8^s + 10°26'21''$); a step corresponds to 500 km s^{-1}. The most significant kinematical structures identified with gap analysis are indicated by different symbols within dashed vertical lines. The bar code at the top of the plot shows the redshift coordinate of the entire sample.

recently passed through the center of A970 (see Lima Neto et al. 2003, for details).

3.3. Abell 1356

Abell 1356 was classified as a Bautz-Morgan II-III morphology and richness class $R = 1$ (Abell et al. 1989), at redshift $z = 0.0698$ (Struble & Rood 1999) based only on 2 velocities. Up to now, the cluster has not been studied except by X-ray observations. A1356 is within the sky area surveyed by the SDSS project which thus provides data, both spectroscopic as photometric, and allowing detailed studies. As seen in Table 1, 8 of the 10 redshift measurement we undertook in the field of A1356 have also being targeted by SDSS.

Jones & Forman (1999) analyzed the *Einstein* IPC X-ray image of A1356. The count rate is 0.0065 s^{-1} in a region of $1h_{50}^{-1}$ Mpc radius giving a luminosity $L_X = 0.429\times10^{44}$ erg s^{-1} in the [0.5–4.5] keV band (notice that they adopted the redshift of $z = 0.1167$, based on Struble & Rood 1987). They did not detect any cooling-flow and they were not able to derive any isocontour map of the X-ray emission.

An analysis of A1356 using ROSAT data was done by Romer et al. (2000) in the context of the SHARC survey. They obtained a total flux $f_X = 51.82 \times 10^{-14}$ erg cm^{-2} s^{-1} in the [0.5−2.0] keV passband, which corresponds to a luminosity $L = 0.11\times10^{44}$ erg s^{-1} assuming a temperature of 2 keV. ROSAT PSPC observations have also been analyzed by Burke et al. (2003), also as part of the SHARC survey. They find that A1356 has a flux $f_X = 57.51 \times 10^{-14}$ erg cm^{-2} s^{-1} in the [0.5−2.0] keV passband and luminosities $L_X = 0.12 \times 10^{44}$ erg s^{-1} in the [0.5−2.0] keV and $L_X = 0.22\times10^{44}$ erg s^{-1} in the [0.3−3.5] keV bands. Both these analyses of ROSAT data were done in an automatic way as part of their pipeline for identifying distant cluster candidates.

Table 2. Kinematical groups projected in the field of A1356.

ID	Redshift range	$\overline{z}$	σ (km s^{-1})	No. of gal
A	$0.020 < z < 0.022$	0.02053	155^{-46}_{+59}	15
B1	$0.067 < z < 0.072$	0.06988	384^{-156}_{+186}	12
B2	$0.078 < z < 0.081$	0.07932	253^{-149}_{+199}	7
C1	$0.102 < z < 0.108$	0.10485	524^{-58}_{+86}	29
C2	$0.115 < z < 0.122$	0.11761	475^{-57}_{+69}	56
C3	$0.126 < z < 0.128$	0.12688	63^{-28}_{+22}	8
D	$0.149 < z < 0.155$	0.15210	491^{-123}_{+117}	25

Figure 7 shows the redshift distribution of galaxies within a square region of side 0.83° centered on A1356, which corresponds to $4\,h_{70}^{-1}$ Mpc at $z = 0.07$, the nominal redshift of the cluster. Data is from the SDSS database added to our own measurements (only 2 new redshifts, see Table 1) and limited to $r = 22$ mag. We iteratively applied the method of weighted gap analysis (see Sect. 3.1) to identifify the main kinematical structures in this distributions. These are denoted by letters in Fig. 7, and their main properties are displayed in Table 2. A1356, nominally at $z \simeq 0.07$, should correspond to structure $B1$, with a velocity dispersion $\sigma_{B1} = 384$ km s^{-1}, which is more characteristic of a sparse group than of a rich cluster of galaxies.

Figure 8 shows the projected positions of galaxies in this same region. As seen, galaxies belonging to $B1$ seem to constitute an elongated SE-W structure, concentrated around the nominal center of A1356. This confirms the reality of this system, although not as a rich cluster of galaxies as it was initially believed, but probably just as a sparse group. The hypothesis that the two kinematical groups could belong to one single structure, with the detected gaps interpreted as due to the incompleteness

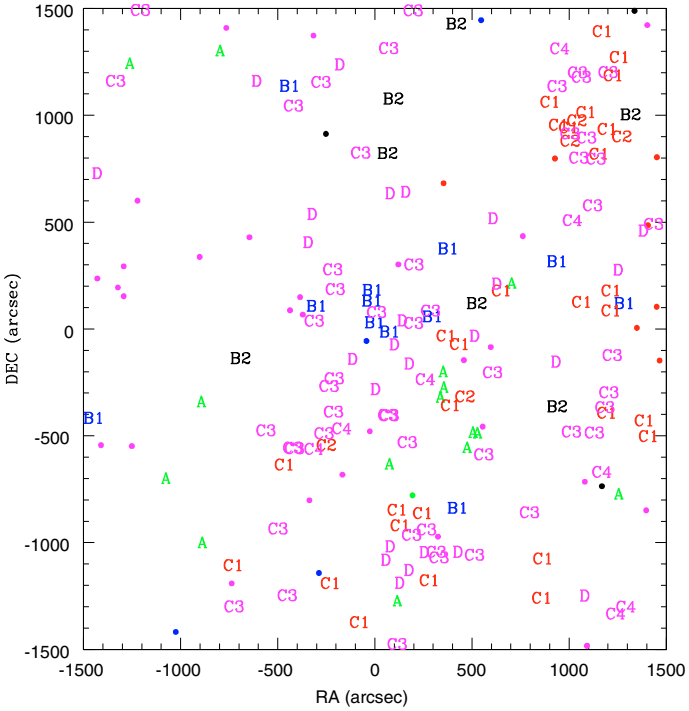

Fig. 8. The projected distribution of galaxies in the field of A1356. Different symbols correspond to different kinematical structures displayed in Fig. 7 and in Table 2. Filled circles are galaxies outside of any kinematical structure. The square region displayed in this figure is centered on the nominal center of A1356 with a side equivalent to $4\,h_{70}^{-1}$ Mpc at $z = 0.07$, the nominal redshift of the cluster.

of the sample, should be disregarded for, given the distance modulus of 37.5, at $z = 0.07$, and assuming $M_r^* = -20.94$, the mean value for rich clusters (Popesso et al. 2006), we get $r^* = 16.6$, well within the completeness limit of the SDSS spectrocopic survey ($r_{\rm lim} \sim 17$).

With the exception of a relatively important concentration at NW of the field displayed in Fig. 8, which should be associated to the Abell cluster A1345 (see below), the other kinematical groups displayed in Table 2 do not appear to be clearly concentrated on their projected surface distribution. It should be stressed that, as for the results displayed in this table, no single one of these groups have velocity dispersion, which could characterize a rich cluster of galaxies, expected to have, typically, $\sigma_{\rm rich\ cluster} > 800$ km s^{-1}. In fact, as seen below (see Fig. 9), no diffuse X-ray emission has been detected in the whole region.

Figure 9 plots the positions of galaxies within the velocity peaks from Table 2 over an X-ray image obtained with ROSAT PSPC in the 0.1–2.4 keV band. We also plot the positions of the clusters in the vicinity of A1356. A1345 is the most evident one at 24 arcmin NW with velocities corresponding to the 3rd and 4th velocity-peak objects of Table 2. This cluster is composed of 2 main structures on the line of sight as shown on the wedge diagrams. The other noticeable clusterings are those of galaxies with $0.087 < z < 0.112$ at the position of A1341 and foreground objects, $0.02 < z < 0.065$ that are part of the HCG 58 (Hickson compact group). Figure 10 shows the redshift wedge diagrams for this sample, in both RA and Dec projections. The projections of an l.o.s view cone with ∼11 arcmin aperture for A1356 (∼$0.9\,h_{70}^{-1}$ Mpc @ $z = 0.07$) are also shown in these figures.

In their study of the distribution of Abell clusters and superclusters, Einasto et al. (1997,2001) defined the *very rich* "Leo-Virgo" supercluster at a mean redshift $z_{\rm SCl} = 0.112$ as composed of 8 Abell clusters, 6 of them with "known distances": A1341 ($z = 0.1049$), A1342 ($z = 0.1061$), A1345 ($z = 0.1095$), A1354 ($z = 0.1178$), A1372 ($z = 0.1126$), and A1356 ($z = 0.117$); and 2 other clusters with only "estimated" distances, A1379 and A1435. However, our analysis above pointed out that A1356 should be considered as just a foreground *group* of galaxies, located at $z = 0.0689$, thus giving no contribution to the Leo-Virgo supercluster. In fact, the field around A1356 seems highly contaminated by background galaxies, with a substantial fraction of them belonging at redshifts of the Leo-Virgo supercluster (groups *C*1, *C*2, and probably *C*3 of Table 2), and this should be the reason for the erroneous description of the cluster. Note that the cluster A1435 has a redshift $z = 0.062$ (NED) and should also be considered as a foreground cluster.

The ROSAT PSPC X-ray image is rather shallow, with an exposure time of 11.7 ks, but it should detect an Abell cluster. To verify that indeed the PSPC could detect extended diffuse emission from a cluster up to $z \approx 0.1$, we selected another Abell cluster that was observed by the PSPC with similar conditions, Abell 2034. It is a $z = 0.113$ cluster classified as a II-III B-M class and richness class 2. Although it is somewhat richer than A1356 (which is classified as richness class 1), it was observed with a shorter exposure time, 8.9 ks compared to 11.7 ks for A1356. We constructed an image for each cluster in exactly the same way and show them in Fig. 11. The difference is striking, so we can conclude that there is no sign of diffuse emission from A1356. If the redshift of A1356 is indeed ∼0.07, as we pointed out above, rather than ∼0.11, the discrepancy between the images would be even stronger.

3.4. Abell 2244

Abell 2244 has a I-II morphology in the Bautz-Morgan classification and a richness class $R = 2$ (Abell et al. 1989). It is a cD or D-galaxy dominated cluster, and its brightest cluster galaxy has an absolute magnitude of −22.0 and a diameter of 98 kpc at the 25 Vmag arcsec^{-2} isophote (Schombert et al. 1989). These authors give a redshift $\overline{z} = 0.0968 \pm 0.0008$ with a dispersion $\sigma = 0.00414$. They note the presence of a very near companion to the cD galaxy at a distance of 3 arcsec (4 kpc) and a velocity difference 50 km s^{-1}, which could be a final stage of merging. They also suggest a subclustering in the line of sight from a set of 18 pairs of galaxies where only one is bound. A second structure has been evidenced by Miller et al. (2005) at a redshift $z = 0.1024$.

The wedge diagrams in RA and Dec of the 417 velocities collected in a 40 arcmin radius (4.64 Mpc) from the NED database completed with our results are displayed in Fig. 12. The positions of the two clusters A2244 and A2245 are represented with ellipses of 3 Mpc in radius perpendicular to the line of sight and 1000 km s^{-1} in radius along the l.o.s. Instead of a double cluster as quoted by Struble & Rood (1999), the two clusters belong to a much larger structure visible in RA and Dec at an average velocity of 28 500 km s^{-1}, which is associated to a supercluster by Einasto et al. (2001), including A2249. The velocity histogram of Fig. 13 shows 2 main peaks corresponding to the main velocities of A2244 and A2245. From the galaxies contained in each ellipse of Fig. 12 we obtain $C_{BI} = 29\,867^{+79}_{-86}$ km s^{-1} and $S_{BI} = 965^{+63}_{-66}$ km s^{-1} (110 galaxies) for A2244 and $C_{BI} = 26\,197^{+102}_{-108}$ km s^{-1} and $S_{BI} = 992^{+57}_{-75}$ km s^{-1} (94 galaxies) for A2245. Rines & Diaferio (2006) obtained for the same clusters respectively $\overline{v} = 29\,890$ km s^{-1}, $\sigma = 981^{+95}_{-74}$ km s^{-1} and $\overline{v} = 26\,022$ km s^{-1}, $\sigma = 952^{+89}_{-70}$ km s^{-1} respectively. For

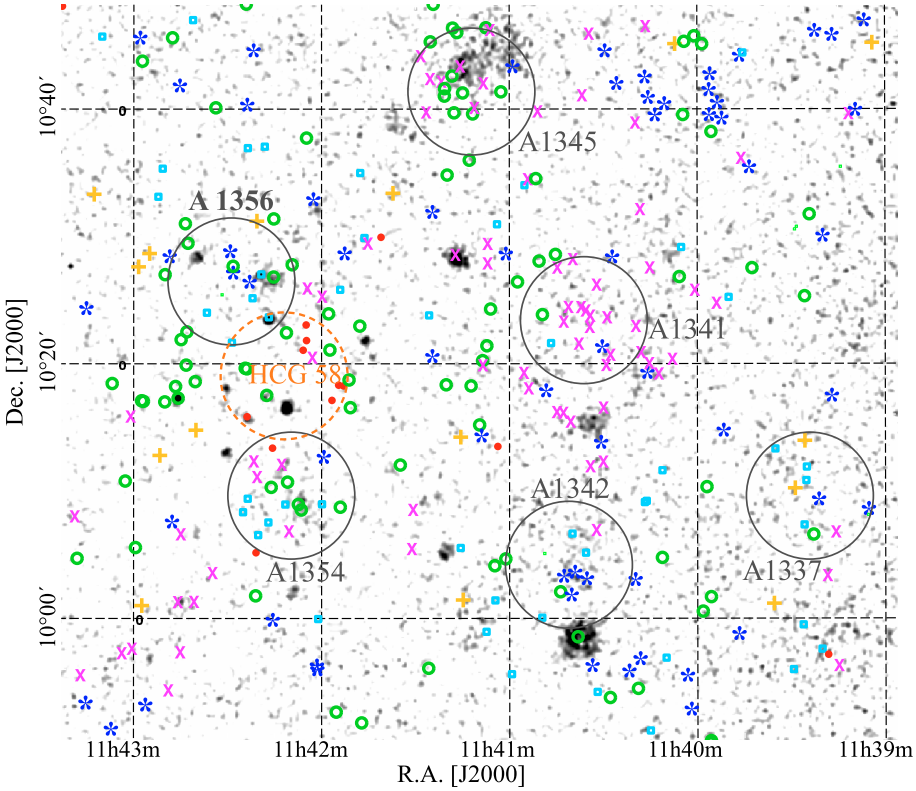

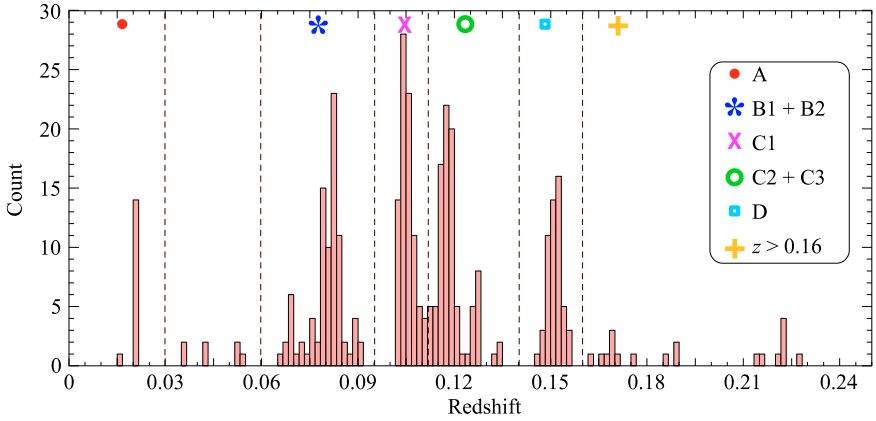

Fig. 9. ROSAT PSPC 0.1–2.4 keV image of the ∼30 arcmin radius around A1356. The large blue circles (4 arcmin radii) correspond to Abell clusters as indicated; the large dashed circle, with 5 arcmin radius, corresponds to HCG 58. The smaller symbols represent galaxies with measured velocities, each symbol corresponding to a redshift range as indicated in the figure. There is no detected diffuse emission associated with A1356.

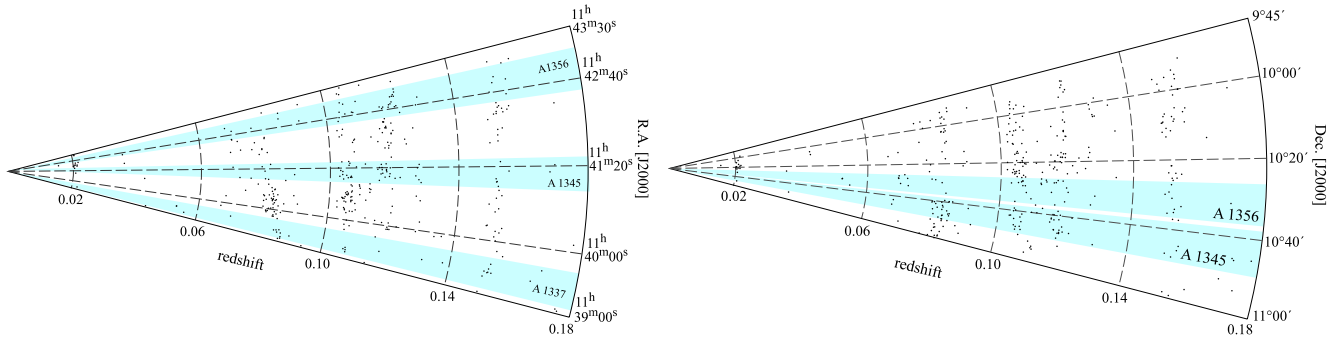

Fig. 10. Wedge diagrams in RA (*left*) and Dec (*right*) for the field of cluster A1356. The shaded areas show the 11.5 arcmin aperture l.o.s view cones for some of the clusters present in the field (see also Fig. 9).

both clusters, there is a very good agreement with Rines & Diaferio (2006), who calculate the velocity dispersion profile within about r_{200} following Danese et al. (1980). Note also the presence of two foregorund structures with prominent peaks at 11 191 km s^{-1} and 18 461 km s^{-1}.

Abell 2244 was observed in X-rays by *Chandra* (Donahue et al. 2005). It is nearly isothermal with $kT = 5.5 \pm 0.5$ keV at every radius < 4 arcmin. Figure 14 shows the gri Sloan image and the *Chandra* contours in the central part of A2244. A small offset between the center of the cD galaxy and the X-ray peak

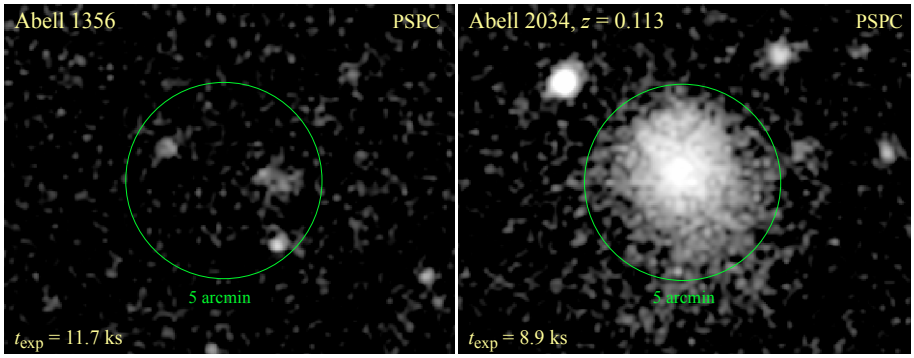

Fig. 11. Comparison between the images of A1356 and A2034. A2034 is a Bautz-Morgan II-III cluster of richness class 2 at $z = 0.113$ observed for 8.9 ks with the ROSAT PSPC. If A1356 were a real cluster, its image should look very similar to the image of A2043.

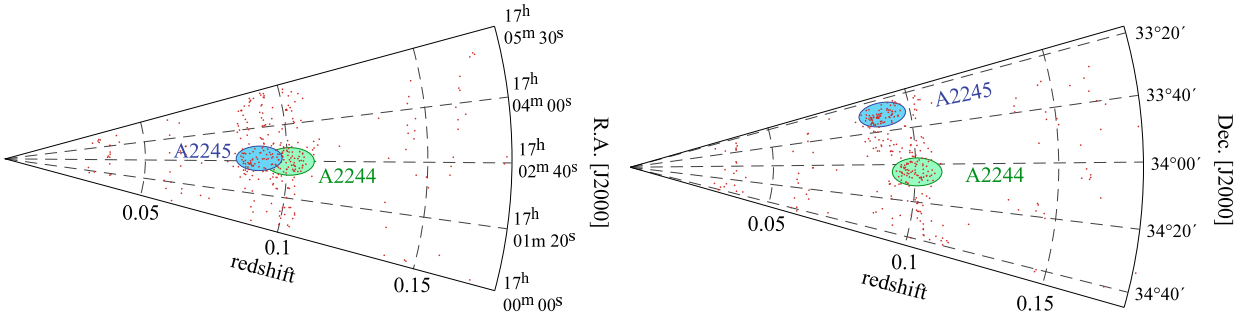

Fig. 12. Wedge diagrams in RA and DEC of the cluster A2244. The ellipses are 3 Mpc in radius, perpendicular to the line of sight and 1000 km s^{-1} in radius along the l.o.s.

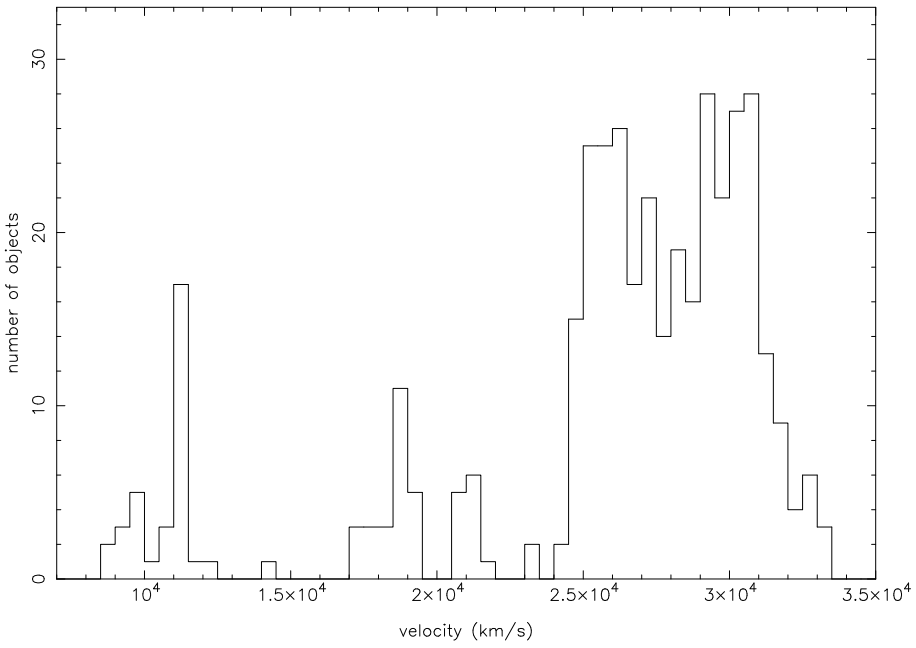

Fig. 13. The radial velocity distribution between 8000 and 35 000 km s^{-1} (step 500 km s^{-1}) of the Abell 2244 and Abell 2245 sample of galaxies.

is visible as a sharp edge on the X-ray image (a cold front or a shock front) about 10 arcsec NE from the center, possibly indicating a movement in that direction. Quoting Donahue et al. (2005), there is no evidence in the X-ray surface brightness map for fossil X-ray cavities produced by a relatively recent episode of AGN heating. No interaction seems to be present between A2244 and A2245.

4. Summary

In this paper we presented a set of 80 new radial velocities in the direction of 4 Abell clusters of galaxies: Abell 376, Abell 970, Abell 1356, and Abell 2244.

For A376 we obtained an improved mean velocity value $\overline{V}_{\rm rec} = 14\,241$ km s^{-1} and velocity dispersion $\sigma = 830$ km s^{-1}. The new data suggest that A376 displays a complex structure with evidence of bimodality in the radial velocity distribution where only the main central core seems to conform to the expected features of a relaxed cluster. The effect of morphological segregation acting locally in the cluster is clearly seen both in the surface distribution of galaxies and in their radial velocity distribution.

For A970, we have $\overline{V}_{\rm rec} = 17\,612$ km s^{-1} and $\sigma = 881$ km s^{-1}. Previous analyses have shown that the cluster has substructures and is out of dynamical equilibrium. The new data presented here confirms this conclusion.

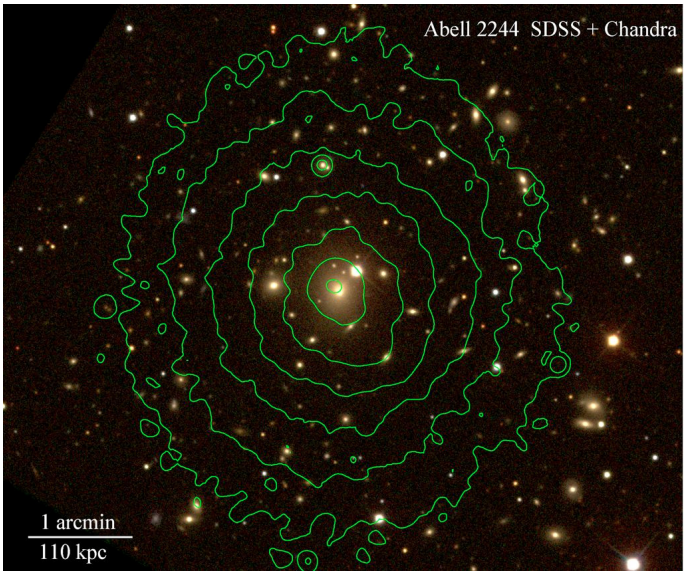

Fig. 14. *Chandra* X-ray contours superimposed to the gri Sloan image in the central part of A2244.

We analyze the cluster A1356 for the first time. We derive a new velocity value $\overline{V}_{\rm rec} = 20\,986$ km s^{-1} with $\sigma = 384$ km s^{-1}. This cluster would not be a member of the "Leo-Virgo" supercluster as well as the cluster A1435 at $\overline{V}_{\rm rec} = 18\,588$ km s^{-1}.

We obtain for A2244 $\overline{V}_{\rm rec} = 29\,867$ km s^{-1} and $\sigma = 965$ km s^{-1} and for A2245 $\overline{V}_{\rm rec} = 26\,197$ km s^{-1} and $\sigma = 992$ km s^{-1}. These two clusters are members of a possible supercluster including A2249. From optical and X-ray data, these A2244 and A2245 show no sign of interaction.

Acknowledgements. We thank the Haute-Provence observatory staff for their assistance during the observations. H.V.C., L.S.J., and G.B.L.N. acknowledge the financial support provided by FAPESP and CNPq. D.P. acknowledges IAG/USP for its hospitality.

References

Abell, G. O., Corwin, H. G., & Olowin, R. P. 1989, ApJS, 70, 1
Adami, C., Biviano, A., & Mazure, A. 1998, A&A, 331, 439
Allen, S. W. 1998, MNRAS, 296, 392
Allen, S. W. 2000, MNRAS, 315, 269
Beers, T. C., Flynn, K., & Gebhardt, K. 1990, AJ, 100, 32
Bird, C. M., & Beers, T. C. 1993, AJ, 105, 159
Burke, D. J., Collins, C. A., Sharples, R. M., Romer, A. K., & Nichol, R. C. 2003, MNRAS, 341, 1093
Cabanela, J. E., Humphreys, R. M., Aldering, G., et al. 2003, PASP, 115, 809
Capelato, H. V., Mazure, A., Proust, D., et al. 1991, A&AS, 90, 355
Capelato, H. V., Proust, D., Lima Neto, G. B., Santos, W. A., & Sodré, Jr. L. 2008, A&A, 492, 345
Carlberg, R. G., Yee, H. K.C., & Ellingson, E. 1997, ApJ, 478, 462
Cypriano, E. S., Lima Neto, G. B., Sodré, Jr. L., Kneib, J. P., & Campusano, L. E. 2005, ApJ, 630, 38
Danese, L., de Zotti, G., & di Tullio, G. 1998, A&A, 82, 322
Donahue, M., Voit, G. M., O'Dea, C. P., Baum, S. A., & Sparks, W. B. 2005, ApJ, 630, L13
Dressler, A. 1980, ApJS, 42, 565
Einasto, M., Tago, E., Jaaniste, J., Einasto, J., & Andernach, H. 1997, A&AS, 123, 119
Einasto, M., Einasto, J., Tago, E., Müller, V., & Andernach, H. 2001, AJ, 122, 2222
Girardi, M., Giuricin, G., Mardirossian, F., Mezzetti, M., & Boschin, W. 1998, ApJ, 505, 74
Jones, C., & Forman, W. 1999, ApJ, 511, 65
Kurtz, M. J., Mink, D. J., Wyatt, W. F., et al. 1991, ASP Conf. Ser., 25, 432
Laine, S., van der Marel, R. P., Lauer, T. R., et al. 2003, AJ, 125, 478
Lauer, T. R., Ajhar, E. A., Byun, Y. I., et al. 1995, AJ, 110, 2622
Leccardi, A., & Molendi, S. 2008, A&A, 486, 359
Lima Neto, G. B., Capelato, H. V., Sodré, Jr. L., & Proust, D. 2003, A&A, 398, 31
Mellier, Y. 1999, ARA&A, 37, 127
Miller, C. J., Nichol, R. C., Reichart, D., et al. 2005, AJ, 130, 968
Mink, D. J., & Wyatt, W. F. 1995, ASP Conf. Ser., 77, 496
Oegerle, W. R., & Hill, J. M. 2001, AJ, 122, 2858
Popesso, P., Biviano, A., Bhringer, H., & Romaniello, M. 2006, A&A, 445, 29
Proust, D., Quintana, H., Mazure, A., et al. 1992, A&A, 258, 243
Proust, D., Mazure, A., Vanderriest, C., Sodré, L., & Capelato, H. V. 1995, A&AS, 114, 565
Proust, D., Cuevas, H., Capelato, H. V., et al. 2000, A&A, 355, 443
Proust, D., Capelato, H. V., Hickel, G., et al. 2003, A&A, 407, 31
Ribeiro, A. L. B., de Carvalho, R. R., Capelato, H. V., & Zepf, S. E. 1998, ApJ, 497, 72
Rines, K., & Diaferio, A. 2006, AJ, 132, 1275
Romer, A. K., Nichol, R. C., Holden, B. P., et al. 2000, ApJS, 126, 209
Schombert, J. M., West, M. J., Zucker, J. R., & Struble, M. F. 1989, AJ, 98, 1999
Sodré, L., Proust, D., Capelato, H. V., et al. 2001, A&A, 377, 428
Sodré, L., Capelato, H. V., Steiner, J. E., & Mazure, A. 1989, AJ, 97, 1279
Stein, P. 1997, A&A, 317, 670
Struble, M. F., & Rood, H. J. 1987, ApJS, 63, 543
Struble, M. F., & Rood, H. J. 1999, ApJS, 125, 35
Tonry, J., & Davis, M. 1979, AJ, 84, 1511